Simple model for surface-enhanced Raman scattering from tilted silver nanorod array substrates

Y.-J. Liu and Y.-P. Zhao
Department of Physics and Astronomy and Nanoscale Science and Engineering Center, University of Georgia, Athens, Georgia 30602, USA
(Received 30 April 2008; published 26 August 2008)

A modified Greenler's model is proposed to interpret surface enhanced Raman scattering (SERS) for molecules adsorbed onto a tilted and aligned Ag nanorod array substrate. This model only considers molecules absorbed on the side walls of the nanorods and the Raman incident and collection configurations. It reveals that when the incident angle increases to an optimal angle, the SERS intensity reaches a maximum. With the increase in the nanorod tilting angles, the maximum SERS intensity almost does not change, but the optimal incident angle increases linearly. The underlayer thin film also plays an important role for SERS enhancement. In addition, the SERS intensity is closely related to the polarization of the excitation light. When the incident angle is smaller than 15°, *s* polarization excites stronger Raman signals; at other incident angles, *p*-polarization excitation contributes more Raman intensity. Those theoretical predictions are qualitatively consistent with our experimental observations.

DOI: 10.1103/PhysRevB.78.075436 PACS number(s): 78.30.−j, 73.40.−c, 68.49.Df, 78.20.Bh

I. INTRODUCTION

Raman spectroscopy (RS) has been proven to be a valuable and accurate tool for process and environmental monitoring,[1–4] chemical and biological sensing,[5–12] and disease diagnosing and biological tissue studying.[13,14] A practical limitation for the application of Raman spectroscopy is the extremely small scattering cross section of the Raman process, which is around 10^{-31} cm^2/molecule, almost 12–14 orders of magnitude lower than fluorescence scattering cross sections.[15] In the 1970s, unexpectedly high Raman signals from pyridine on a rough silver electrode were discovered, and this so-called "surface-enhanced Raman scattering" (SERS) showed a great promise in applications of Raman spectroscopy.[16] It has been reported that unexpectedly large scattering cross sections on the order of 10^{-16} cm^2/molecule, corresponding to enhancement factors of about 14 orders of magnitude compared with normal nonresonant RS, could give the sensitivity of a single molecule.[17–21] So far, two primary mechanisms are believed to be responsible for such a huge Raman enhancement: a long-range classical electromagnetic (EM) effect and a short-range chemical (CHEM) effect.[22–26] These two mechanisms contribute simultaneously to the overall enhancement. Since there is no chemical effect in SERS in most molecules,[27] the EM mechanism is proposed to contribute the most to the observed intensity enhancement. The intensity enhancement attributed to the SERS EM mechanism is due primarily to the enhancement of the local electric field. A critical aspect of SERS is the requirement of a specific surface morphology to specify the local electric field and to achieve reproducible and high levels of enhancement. A large variety of nanostructures have been found to manifest the SERS effect, including rough metallic surfaces by chemical etching,[28] island films,[29] aggregates of colloidal particles,[20,21] high aspect ratio of Ag and Au nanorods and nanowires fabricated by chemical and electrochemical methods,[30,31] or regular nanoparticle arrays prepared by nanosphere lithography[32] or electron-beam lithography.[33] Unfortunately, many of these fabrication methods are either expensive or time consuming and fail to produce reproducible substrates with the correct nanostructure to provide maximum SERS enhancements.

The oblique angle deposition (OAD) technique has been recently employed to produce Ag nanorod arrays which were shown to make excellent SERS substrates.[34–37] OAD is a physical vapor deposition technique in which the incident metal vapor is deposited on a substrate at a large incident angle (>70°) with respect to the surface normal of the substrate.[38–40] Due to the self-shadowing effect and surface diffusion, nanocolumnar structures can be formed. We have recently demonstrated that a Ag nanorod array fabricated by OAD, with length of ~900 nm, diameter of ~100 nm, and tilting angle of ~73°, can achieve a SERS enhancement factor of $>10^8$ for the molecular probe trans-1, 2-bis(4-pyridyl) ethane (BPE).[34,37,41] These substrates have a relatively good uniformity and reproducibility and have been demonstrated to distinguish different viruses and different strains of viruses.[9,41,42] Figures 1(a) and 1(b) show the typical top view and cross-section scanning electron microscopy (SEM) images of this particular Ag nanorod array substrate. The OAD

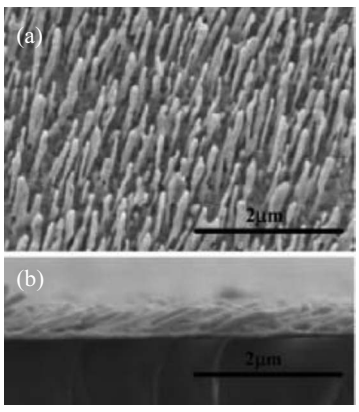

FIG. 1. (a) A top view SEM image and (b) a cross-section SEM image of Ag nanorod array substrate fabricated by the OAD technique.

technique can offer a flexible, easy, and inexpensive way to fabricate Ag nanorod arrays for high sensitivity SERS applications.

From our experimental studies, the SERS spectrum obtained from Ag nanorod array substrates has the following three unique characteristics: (1) incident angle dependence (the SERS intensity reaches the maximum value when the excitation laser incident at an angle around 45° when the OAD deposition angle is 86° with a backscattering collection configuration[36]), (2) substrate reflectivity dependence (when Ag nanorods are deposited onto 500 nm thick Ag film substrate, the SERS signal was about 10^3 times higher than that obtained from Ag nanorods directly deposited onto a glass substrate[34]), and (3) polarization dependence (with a normal-incidence excitation and the backscattering collection configuration, the *s*-polarization SERS signal where the excitation *E* field is perpendicular to nanorod long axis is higher than that of the *p* polarization[37]). Clearly these three characteristics all relate to the excitation configuration and the structure of the substrates. In most SERS studies, these characteristics are hardly studied. There is no existing theory to predict these behaviors for nanorod array SERS substrates. However, a similar theory has been proposed to describe the Raman spectrum of a molecule adsorbed on a flat surface. Greenler's model is proposed to explain the effects of the incident angles, the collecting angles, and the polarization dependence of Raman scattering by a molecule adsorbed on a planar surface through classical electrodynamics.[43] In this model, the Raman molecules are treated as oscillating dipoles. The primary field E_P felt by the molecule is the sum of the incident and reflected fields, and this field induces an oscillating dipole in the molecule. The oscillating dipole can be considered as a point-source emitting Raman radiation. The sum of the directly emitted field and the field suffering a single reflection from the surface is the secondary or scattered field E_R. The Raman intensity is proportional to the mean square of total scattered field $\langle E_R \rangle^2$. Here, the incident angle and incident light polarizations determine the magnitude of the primary field. The strength and orientation of the induced dipole depend on the mode symmetry of the molecule considered and its scattering cross section. The orientation of the induced dipole also determines the variation in scattered intensity with observation angle. This model gave some correct explanations for the Raman behavior of a molecule adsorbed on a planar surface.[44] Thus, it naturally extends this model to SERS behavior of nanorod array substrate. However, the nanorod substrate is not a planar substrate. Based on our experimental results and conditions, we have made several further assumptions and proposed a modified Greenler's model to explain the dependence of incident angle, nanorod tilting angle, the polarization, and reflection of the substrate of the SERS intensity from BPE molecules adsorbed onto Ag nanorods fabricated by the OAD method.

II. MODIFIED GREENLER'S MODEL

For Raman scattering by a molecule adsorbed on a planar surface, the behaviors of both the incident and scattering fields near this molecule have been considered. Due to the high porosity and anisotropy of the Ag nanorod, we cannot treat the substrate as a planar surface as in the standard Greenler's model. Based on the experimental geometry, we make the following assumptions.

(1) The surface of the nanorod can be simply treated as a planar surface by neglecting the diffraction effect, and we only consider Raman scattering from a single nanorod. This is a very crude assumption. The length of nanorods (~800–900 nm) is longer than the wavelength of the excitation source (785 nm), while the diameter (~100 nm) is smaller than the wavelength. The multiple-scattering effects within adjacent nanorods need to be taken into consideration in the future since the separation and diameter of the nanorods are much smaller than the wavelength of the excitation source, and the Ag nanorod surface is rough.[45]

(2) The BPE molecules are usually adsorbed on the sides and top of the nanorods and are also oriented perpendicular to the nanorod surface. According to Yang *et al.*,[46] the long axis of the BPE molecule is always perpendicular to the adsorbed surface. The gap between the Ag nanorods is approximately 177 nm, which is much larger than the diameter of the BPE molecules; and the nanorods have a large aspect ratio (~10). In the development of a scattering model, the BPE molecule is treated as a dipole on the Ag nanorod surface, which is perpendicular to the long axis of the nanorod.

(3) To be simple, the SERS effect of molecules on the top of Ag nanorods can be neglected compared to the SERS intensity of the molecules on the side surface of Ag nanorods, i.e., we do not consider the lightening-rod effect. We set g as the E-field enhancement averaged over the surface of the Ag nanorod and E_P as the magnitude of the primary field which is the sum of the incident and reflected fields by Ag nanorod and Ag thin-film surface. The enhanced local electric field can be written as $E_l = gE_P$. The molecules adsorbed at the surface of the Ag nanorod will therefore be excited by this local field E_l. The Raman-scattered fields E_R are the result of the radiation by oscillating molecular dipoles and can be expressed as $E_R \propto \alpha E_l \sin\varphi$, where α is the polarizability of the molecules and φ is the radiation angle from the dipole. The Raman-scattered fields will be reflected by the Ag nanorod. The sum of the Raman-scattered field and its reflection from the Ag nanorod called secondary field will be further enhanced by the Ag nanorods in exactly the same manner as the primary field is. That is, the Ag nanorod can scatter light at the Raman-shifted wavelength with a field enhanced by a factor g'. So, the amplitude of the SERS-scattered field will be $E_{\mathrm{SERS}} \propto \alpha g g' E_P$, and the average SERS intensity $I_{\mathrm{SERS}} \propto |\alpha|^2 |gg'|^2 I_P$. Since $I_P \propto I_0$, where I_0 is the incident intensity, the above equation shows that the SERS intensity is proportional to the incident intensity, which is consistent with our experimental observation.[9,41,42] If we set $I_{\mathrm{SERS}} = GI_P$, where G is defined as "SERS enhancement factor," then $G \propto |\alpha|^2 |gg'|^2$.[25] If the primary electric field E_P can be decomposed as the field $E_{P\perp}$ that is perpendicular to the nanorod long axis and the field $E_{P\parallel}$ that is parallel to the nanorod long axis, the average SERS intensity can be written as $I_{\mathrm{SERS}} = G_\perp n_\perp E_{P\perp}^2 + G_\parallel n_\parallel E_{P\parallel}^2$, where $n_\perp$ and $n_\parallel$ are the numbers of the molecules on the side and the top surface of nanorod and $G_\perp$ and $G_\parallel$ are the SERS enhancement factors at

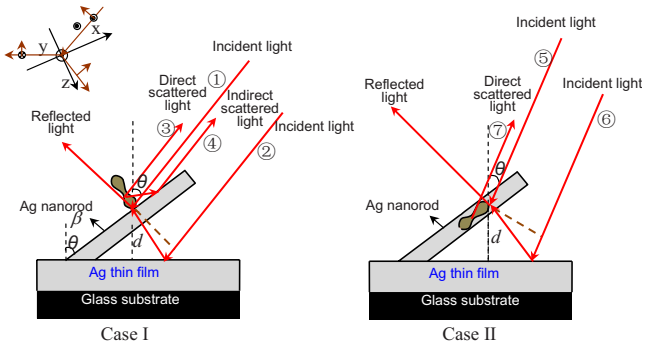

FIG. 2. (Color online) A schematic illustration of the modified Greenler's model. (a) Case I—the dipole is in the incident plane; (b) Case II—the dipole is perpendicular to the incident plane. All the induced dipoles are perpendicular to the nanorod.

the directions perpendicular and parallel to nanorod long axis, respectively. If we assume that the BPE molecules are uniformly adsorbed on the Ag nanorod surface, for a single Ag nanorod, the ratio of BPE molecules on the side and the tip of Ag nanorod surface is $n_\perp/n_\parallel = S_{\text{side}}/S_{\text{top}} = 2l/r$, where l is the length of the nanorod and r is the radius of the nanorod. According to our experiments, $l \approx 900$ nm, $r \approx 50$ nm, and $n_\perp/n_\parallel = 36$. In addition, from the UV-visible polarized extinction spectra, the longitude-mode plasmon peak of the Ag nanorod array is around 1056 nm and the transverse-mode plasmon peak is located at about 357 nm,[37] while the Raman excitation laser wavelength is 785 nm. This means that the SERS observed in the experiments is not near the surface-plasmon resonance frequency. Under this condition, a rough numerical calculation using discrete dipole approximation (DDA) method has shown that $G_\perp/G_\parallel \approx 1$. Thus the main contribution of the average SERS intensity can be simplified as $I_{\text{SERS}} \approx G_\perp n_\perp E_{P\perp}^2$, i.e., the contribution to the SERS intensity of the molecules adsorbed on the tip of Ag nanorod surface can be neglected compared with the contribution of the molecules on the side surface of the Ag nanorod.

(4) In the experimental setup, a backscattering collecting configuration is employed, which means that the exciting direction and the collecting directions have 180 phase difference. Thus, in the proposed model, we also consider such a configuration.

Since any oscillating motion of the dipole can be decomposed into two orthogonal motions which are parallel and perpendicular to the incident plane, respectively, we can simply consider two cases. The details of the model are depicted in Fig. 2. Case I—the dipole is parallel to the incident plane; case II—the dipole is perpendicular to the incident plane. For case I, as shown in Fig. 2(a), the incident light beam ① hits the molecule and reflects from the surface of nanorod and another incident light beam ② hits the Ag thin film and reflects back to the molecule. The incident beam ① the reflected beam from the nanorod, and the reflection of the beam ② all contribute to the primary field for the molecules on the nanorod and excite the molecules vibrating and radiating. One part of the radiation or the scattered light ③ from the molecule dipole directly goes to a detector; the other part of the scattered light ④ hits the nanorod and is reflected by the surface of nanorod and then goes into the detector. For case II, as shown in Fig. 2(b), the incident light beam ⑤ hits the molecule and the incident light beam ⑥ hits the Ag thin film and reflected by the film and then passes through the molecule. In this case, the incident beam ⑤ and the reflection of beam ⑥ contribute to the primary field. The scattered light ⑦ from the molecule dipole is directly collected by the detector, and no scattered light reflecting from the nanorod enters the detector since the collection direction is perpendicular to molecular vibrating direction in this case. The total Raman intensity is the sum of the scattering intensities in case I and case II. In both cases, since the tilting of the nanorod breaks the symmetry, if the excitation light incidents from right or left of the substrate surface normal, θ is positive or negative. The nanorod tilting angle is β with respect to the normal of substrates.

A. Primary fields

Assuming that the fields E_{is} and E_{ip} are s- and p-polarized components of the incident light, the fields E_{rs} and E_{rp} are s- and p-polarized components of the reflected light from the Ag nanorod, and the fields E'_{rs} and E'_{rp} are the s- and p-polarized components of the reflected light beams from the Ag thin film, respectively. The total phase shifts of the beam reflected by the Ag nanorod surface compared with incident beam ① for the s- and p-polarized components are δ_s and δ_p, $\delta_{s,p} = \delta_r$, where δ_r is the phase shift of the reflected beam of beam ①. The phase shifts of the beam reflected by Ag thin film compared with incident beam ① for the s- and p-polarized components are $\delta_{s'}$ and $\delta_{p'}$, $\delta_{s',p'} = \delta_{r'} + \delta_d$, where $\delta_{r'}$ is the phase shift of the reflected beam of beam ②. The phase shift due to the optical path difference between beams ① and ② is $\delta_d = 2\pi\Delta/\lambda$ and $\Delta = d(1+\cos 2\theta)/\cos\theta$ where d is the vertical distance from the molecule to the Ag thin film. In our experiments, the length of Ag nanorod is around 900 nm and the nanorod tilting angle is $\sim 70°$, so d varies from 0 to 308 nm. The reflected fields can be calculated by the Fresnel equations,

$$r_s = E_{rs}/E_{is} = \frac{\cos\theta_i - (\tilde{n}_2^2 - \sin^2\theta_i)^{1/2}}{\cos\theta_i + (n_2^2 - \sin^2\theta_i)^{1/2}}, \tag{1}$$

$$r_p = E_{rp}/E_{ip} = \frac{\tilde{n}_2^2\cos\theta_i - (\tilde{n}_2^2 - \sin^2\theta_i)^{1/2}}{\tilde{n}_2^2\cos\theta_i + (\tilde{n}_2^2 - \sin^2\theta_i)^{1/2}}, \tag{2}$$

where θ_i is the incident angle with respect to the direction perpendicular to Ag nanorod, $\theta_i = \pi/2 - \beta + \theta$. The reflected fields from Ag thin film are given by the following equations:

$$r'_s = E'_{rs}/E_{is} = \frac{\cos\theta - (\tilde{n}_2^2 - \sin^2\theta)^{1/2}}{\cos\theta + (\tilde{n}_2^2 - \sin^2\theta)^{1/2}}, \tag{3}$$

$$r'_p = E'_{rp}/E_{ip} = \frac{\tilde{n}_2^2 \cos\theta - (\tilde{n}_2^2 - \sin^2\theta)^{1/2}}{\tilde{n}_2^2 \cos\theta + (\tilde{n}_2^2 - \sin^2\theta)^{1/2}}, \tag{4}$$

where r_s and r_p are the reflectivity of s- and p-polarized components by the Ag nanorod surface and r'_s and r'_p are the reflectivity of the s- and p-polarized components by the Ag thin film.

Let

$$R_s = |r_s|^2, \quad R_p = |r_p|^2, \tag{5}$$

$$R'_s = |r'_s|^2, \quad R'_p = |r'_p|^2. \tag{6}$$

The reflection phase shifts of s-polarization and p-polarization E fields from the Ag nanorod and the Ag thin film are

$$\delta_s = \tan^{-1}[\mathrm{Im}(r_s)/\mathrm{Re}(r_s)], \quad \delta_p = \tan^{-1}[\mathrm{Im}(r_p)/\mathrm{Re}(r_p)], \tag{7}$$

$$\delta'_s = \tan^{-1}[\mathrm{Im}(r'_s)/\mathrm{Re}(r'_s)], \quad \delta'_p = \tan^{-1}[\mathrm{Im}(r'_P)/\mathrm{Re}(r'_P)]. \tag{8}$$

The primary field at the nanorod surface is the sum of the incident and reflected fields from Ag nanorod and the reflected electric field from the Ag thin film, i.e., $\vec{E}_P = \vec{E}_i + \vec{E}_r + \vec{E}'_r e^{i\delta_d}$. We set the direction along the nanorods as the x axis as shown in Fig. 2(a), the direction perpendicular to the incident plane and pointing inside as the y axis, and the direction perpendicular to the nanorod surface as z axis. For case I, the components, E_x, E_y, and E_z of the primary field in Cartesian coordinates can be written as

$$E_x = -E_{ip}\sin(\theta-\beta) + E_{rp}\sin(\theta-\beta) - \tilde{n}_2^2 E'_{rp}\cos(\theta+\beta), \tag{9}$$

$$E_y = E_{is} + E_{rs} + \tilde{n}_2^2 E'_{rs}, \tag{10}$$

$$E_z = E_{ip}\cos(\theta-\beta) + E_{rp}\cos(\theta-\beta) - \tilde{n}_2^2 E'_{rp}\sin(\theta+\beta). \tag{11}$$

Thus, the intensity of the primary field for case I is

$$\langle E_x^2\rangle = \langle E_{ip}^2\rangle\Bigg[\sin^2(\theta-\beta) + R_p\sin^2(\theta-\beta) + \tilde{n}_2^4 R'_p\cos^2(\theta+\beta) - 2R_p^{1/2}\sin^2(\theta-\beta)\cos\delta_p - 2\tilde{n}_2^2 R_p'^{1/2}\sin(\theta-\beta)$$
$$\times\cos\left(\delta'_p + \frac{2\pi}{\lambda}\Delta\right)\cos(\theta+\beta) + 2\tilde{n}_2^2 R_p^{1/2} R_p'^{1/2}\sin(\theta-\beta)\cos\left(\delta'_p + \frac{2\pi}{\lambda}\Delta - \delta_p\right)\cos(\theta+\beta)\Bigg], \tag{12}$$

$$\langle E_z^2\rangle = \langle E_{ip}^2\rangle\Bigg[\cos^2(\theta-\beta) + R_p\cos^2(\theta-\beta) + \tilde{n}_2^4 R'_p\sin^2(\theta+\beta) + 2R_p^{1/2}\cos^2(\theta-\beta)\cos\delta_p + 2\tilde{n}_2^2 R_p'^{1/2}\cos(\theta-\beta)$$
$$\times\cos\left(\delta'_p + \frac{2\pi}{\lambda}\Delta\right)\sin(\theta+\beta) + 2\tilde{n}_2^2 R_p^{1/2} R_p'^{1/2}\cos(\theta-\beta)\cos\left(\delta'_p + \frac{2\pi}{\lambda}\Delta - \delta_p\right)\sin(\theta+\beta)\Bigg], \tag{13}$$

$$\langle E_y^2\rangle = \langle E_{is}^2\rangle\left[1 + R_s + \tilde{n}_2^4 R'_s + 2R_s^{1/2}\cos\delta_s + 2\tilde{n}_2^2 R_s'^{1/2}\cos\left(\delta'_s + \frac{2\pi}{\lambda}\Delta\right) + 2\tilde{n}_2^2 R_s^{1/2} R_s'^{1/2}\cos\left(\delta'_s + \frac{2\pi}{\lambda}\Delta - \delta_s\right)\right]. \tag{14}$$

Moreover, the polarized primary intensity is

$$\langle E_p^2\rangle = \langle E_x^2\rangle + \langle E_z^2\rangle = \langle E_{ip}^2\rangle\Bigg[1 + R_p + \tilde{n}_2^4 R'_p + 2R_p^{1/2}\cos\delta_p\cos 2(\theta-\beta) + 2\tilde{n}_2^2 R_p'^{1/2}\cos\left(\delta'_p + \frac{2\pi}{\lambda}\Delta\right)\sin 2\beta$$
$$+ 2\tilde{n}_2^2 R_p^{1/2} R_p'^{1/2}\sin 2\theta\cos\left(\delta'_p + \frac{2\pi}{\lambda}\Delta - \delta_p\right)\Bigg], \tag{15}$$

$$\langle E_s^2\rangle = \langle E_y^2\rangle = \langle E_{is}^2\rangle\left[1 + R_s + \tilde{n}_2^4 R'_s + 2R_s^{1/2}\cos\delta_s + 2\tilde{n}_2^2 R_s'^{1/2}\cos\left(\delta'_s + \frac{2\pi}{\lambda}\Delta\right) + 2\tilde{n}_2^2 R_s^{1/2} R_s'^{1/2}\cos\left(\delta'_s + \frac{2\pi}{\lambda}\Delta - \delta_s\right)\right]. \tag{16}$$

In case II, because there are no reflections from Ag nanorod surface, $R_s = R_p = 0$ in Eqs. (15) and (16), the polarized primary intensity can be written as

$$\langle E_p^2\rangle = \langle E_x^2\rangle + \langle E_z^2\rangle = \langle E_{ip}^2\rangle\left[1 + \tilde{n}_2^4 R'_p + 2\tilde{n}_2^2 R_p'^{1/2}\cos\left(\delta'_p + \frac{2\pi}{\lambda}\Delta\right)\sin 2\beta\right], \tag{17}$$

$$\langle E_s^2\rangle = \langle E_y^2\rangle = \langle E_{is}^2\rangle\left[1 + \tilde{n}_2^4 R'_s + 2\tilde{n}_2^2 R_s'^{1/2}\cos\left(\delta'_s + \frac{2\pi}{\lambda}\Delta\right)\right]. \tag{18}$$

B. Secondary fields

The radiation from the molecule dipole is the primary source for the secondary field. The relationship between the scattering field and the incident field can be expressed as[47]

$$\begin{pmatrix} E_{p\_\mathrm{sca}} \\ E_{s\_\mathrm{sca}} \end{pmatrix} = \chi \begin{pmatrix} \sin\varphi & 0 \\ 0 & 1 \end{pmatrix} \begin{pmatrix} E_{p\_\mathrm{inc}} \\ E_{s\_\mathrm{inc}} \end{pmatrix}, \tag{19}$$

$$E_{p\_\mathrm{sca}} = \chi E_{p\_\mathrm{inc}} \sin\beta, \tag{20}$$

$$E_{s\_\mathrm{sca}} = \chi E_{s\_\mathrm{inc}}, \tag{21}$$

where $\chi=(\exp(ik_0r)/r)k_0\mu$, r is the distance between the dipole and the observer (or the detector), $k_0=2\pi/\lambda$, and μ is the molecular polarizability. Here, to be simplified, we set $\chi=1$, thus $\langle E^2_{p\_\mathrm{sca}}\rangle=\langle E^2_{p\_\mathrm{inc}}\rangle\sin^2\varphi$ and $\langle E^2_{s\_\mathrm{sca}}\rangle=\langle E^2_{s\_\mathrm{inc}}\rangle$.

In case I, the dipole is perpendicular to the nanorod and is also parallel to the incident plane. We assume that E_d is the directly scattered field from the dipole and E_r is the field scattered from the dipole toward the nanorod and then reflected toward the detector. The components of the total Raman scattering fields E_I recorded by the detector are $E_{\mathrm{I}x}$, $E_{\mathrm{I}y}$, and $E_{\mathrm{I}z}$,

$$\langle E_d^2\rangle = \langle E_p^2\rangle \sin^2\theta_i, \tag{22}$$

$$E_{\mathrm{I}x} = -E_d\cos\theta_i - E_r\cos\theta_i, \tag{23}$$

$$E_{\mathrm{I}z} = -E_d\sin\theta_i - E_r\sin\theta_i, \tag{24}$$

$$E_\mathrm{I}^2 = E_{\mathrm{I}x}^2 + E_{\mathrm{I}z}^2 = E_d^2 + E_r^2 + 2E_dE_r, \tag{25}$$

$$\langle E_\mathrm{I}^2\rangle = \langle E_{ip}^2\rangle \times A = \langle E_{ip}^2\rangle \left[1 + \tilde{n}_2^4 R_p' + 2\tilde{n}_2^2 R_p'^{1/2}\cos\left(\delta_p' + \frac{2\pi}{\lambda}\Delta\right)\sin 2\beta\right]\sin^2\theta_i(1 + R_p + 2R_p^{1/2}\cos\delta_p), \tag{26}$$

where

$$A = \left[1 + \tilde{n}_2^4 R_p' + 2\tilde{n}_2^2 R_p'^{1/2}\cos\left(\delta_p' + \frac{2\pi}{\lambda}\Delta\right)\sin 2\beta\right]\sin^2\theta_i(1 + R_p + 2R_p^{1/2}\cos\delta_p). \tag{27}$$

For case II, the dipoles are not only perpendicular to the nanorod but also perpendicular to the incident plane. The total Raman scattering fields going into the detector are E_II,

$$E_\mathrm{II} = E_d, \tag{28}$$

$$\langle E_\mathrm{II}^2\rangle = \langle E_d^2\rangle = \langle E_s^2\rangle = \langle E_{is}^2\rangle \times B = \langle E_{is}^2\rangle\left[1 + \tilde{n}_2^4 R_s' + 2\tilde{n}_2^2 R_s'^{1/2}\cos\left(\delta_s' + \frac{2\pi}{\lambda}\Delta\right)\right], \tag{29}$$

where

$$B = \left[1 + \tilde{n}_2^4 R_s^2 + 2\tilde{n}_2^2 R_s'^{1/2}\cos\left(\delta_s' + \frac{2\pi}{\lambda}\Delta\right)\right]. \tag{30}$$

Therefore, considering both case I and case II, the total Raman scattering field $E_{R\ \mathrm{total}}$ can be written as

$$\begin{aligned}\langle E_{R\ \mathrm{total}}^2\rangle &= \langle E_\mathrm{I}^2\rangle + \langle E_\mathrm{II}^2\rangle = \langle E_{ip}^2\rangle \times A + \langle E_{is}^2\rangle \times B \\ &= \langle E_{ip}^2\rangle\left[1 + R_p + \tilde{n}_2^4 R_p' + 2R_p^{1/2}\cos\delta_p\cos 2(\theta-\beta) + 2\tilde{n}_2^2 R_p'^{1/2}\cos\left(\delta_p' + \frac{2\pi}{\lambda}\Delta\right)\sin 2\beta + 2\tilde{n}_2^2 R_p^{1/2} R_p'^{1/2}\sin 2\theta\right. \\ &\quad \left.\times\cos\left(\delta_p' + \frac{2\pi}{\lambda}\Delta - \delta_p\right)\right](1 + R_p + 2\sqrt{R_p}\cos\delta_p)\cos^2(\theta-\beta) + \langle E_{is}^2\rangle\left[1 + \tilde{n}_2^4 R_s' + \tilde{n}_2^2 2R_s'^{1/2}\cos\left(\delta_s' + \frac{2\pi}{\lambda}\Delta\right)\right].\end{aligned} \tag{31}$$

This equation reveals that the SERS intensity from nanorod array depends on the incident angle, the nanorod tilting angle, the polarization of incident light, and the reflection of the substrate. In the following, we will give a detailed discussion.

III. DISCUSSIONS

A. Effect of incident and tilting angles

From Eq. (31), SERS intensity clearly depends on the incident angles and nanorod tilting angles. For case I, only

the p-polarized light can induce dipole oscillation. Due to the tilting of the nanorods, only dipoles on one side of the nanorods can be excited as shown in Fig. 2(a). For case II, only the s-polarized incident light can induce dipole radiations. When the incident light is unpolarized light, $\langle E_{is}^2\rangle = \langle E_{ip}^2\rangle = \langle E_i^2\rangle/2$. Assuming that the nanorod tilting angle β is fixed and η_{Raman} is the ratio of the total Raman scattering power to incident light power called the relative Raman intensity, then the relative Raman intensity η_{Raman} excited by an unpolarized light can be expressed as

$$\eta_{\text{Raman}} = \langle E_{R\ \text{total}}^2\rangle/\langle E_i^2\rangle = \frac{1}{2}(A+B)$$
$$= \frac{1}{2}\left\{\left[1 + R_p + \tilde{n}_2^4 R_p' + 2R_p^{1/2}\cos\delta_p \cos 2(\theta-\beta) + 2\tilde{n}_2^2 R_p'^{1/2}\cos\left(\delta_p' + \frac{2\pi}{\lambda}\Delta\right)\sin 2\beta + 2\tilde{n}_2^2 R_p^{1/2} R_p'^{1/2}\sin 2\theta\right.\right.$$
$$\left.\left.\times\cos\left(\delta_p' + \frac{2\pi}{\lambda}\Delta - \delta_p\right)\right](1 + R_p + 2\sqrt{R_p}\cos\delta_p)\cos^2(\theta-\beta) + \left[1 + \tilde{n}_2^4 R_s' + \tilde{n}_2^2 2R_s'^{1/2}\cos\left(\delta_s' + \frac{2\pi}{\lambda}\Delta\right)\right]\right\}. \quad (32)$$

From Eq. (32), the relationship between the relative Raman intensity η_{Raman} and the incident angles can be calculated. In the calculation, we set the wavelength of incident light $\lambda = 785$ nm, the index of refraction $\tilde{n}_1 = 1$ for air, and the complex refractive index of Ag $\tilde{n}_2 = 0.03 + 5.242i$ (for $\lambda = 785$ nm) where $n_2 = 0.03$ and $k_2 = 5.242$. Figure 3 plots the relative Raman intensity η_{Raman} as a function of the incident angle θ for nanorod tilting angles from 63° to 72°. The Raman intensity increases with the incident angle initially and then reaches a maximum. With a further increase in the incident angle, the Raman intensity decreases. The incident angle that results in the maximum Raman intensity is denoted as the optimal angle θ_0. This result is qualitatively consistent with our experimental observation.[36] For example, in our experiments, the deposition angle was 86°, the tilting angle of the Ag nanorods was $\beta = 71.3° \pm 4°$, and the optimal angle we measured was around $\theta_0 = 45°$. According to Fig. 3, the modified Greenler's model gives $\theta_0 = 47°$ for $\beta = 71°$, which is consistent with the experiment. Figure 3 also shows that the maximum Raman intensity is almost the same for the Ag nanorod array substrates with different nanorod tilting angles, and the curves shift to right with the increase in the nanorod tilting angles, which means that the optimal incident angle θ increases with the increase in nanorod tilting angles β. Figure 4 plots the relationship of θ_0 versus β; the optimal angles θ_0 change linearly from 40° to 49° when the nanorod tilting angles β change from 63° to 72° in Eq. (32).

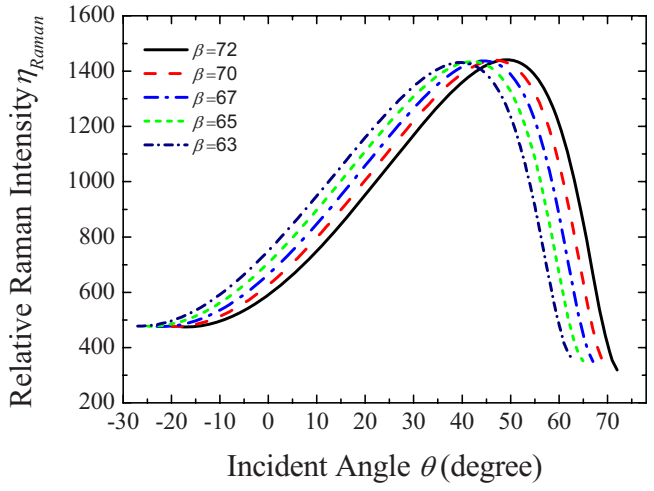

FIG. 3. (Color online) The relative Raman intensity η_{Raman} as a function of the incident angle θ calculated from the modified Greenler's model for a Ag nanorod SERS substrate. The underlayer substrate is Ag, the excitation light is unpolarized, and the nanorod tiling angles are $\beta = 63°$ (navy short-dashed curve), 65° (green short-dashed curve), 67° (blue dashed-dotted curve), 70° (red dashed curve), and 72° (black solid curve), respectively.

B. Effect of the underlayer thin film

As demonstrated by the experiments, a Ag thin-film layer underneath the Ag nanorod array substrate plays an important role to enhance the Raman intensity. In Eq. (32), the role of this thin-film layer is reflected by R_s' and R_p', the reflectivity from the underlayer film. To see how different underlayers affect the Raman intensity, we consider three different cases: (a) Ag thin film, (b) glass substrate, and (c) freestand-

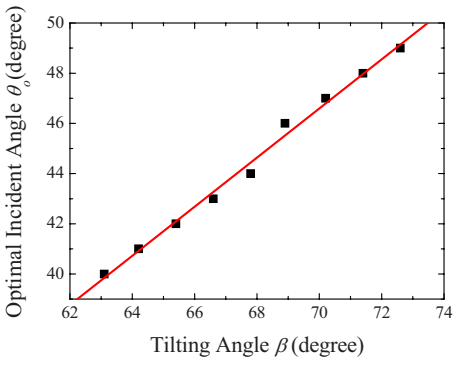

FIG. 4. (Color online) The optimal incident angle θ_0 as a function of Ag nanorod tilting angle β under unpolarized excitation light.

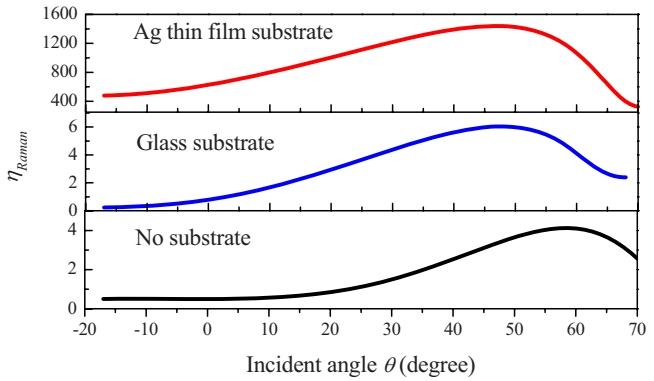

FIG. 5. (Color online) The relative Raman intensity η_{Raman} as a function of incident angle θ for different underlayer thin films: (a) Ag thin film (red solid curve); (b) glass substrate (blue solid curve); and (c) no substrate (black solid curve). The nanorod tilting angle is fixed, $\beta=70°$.

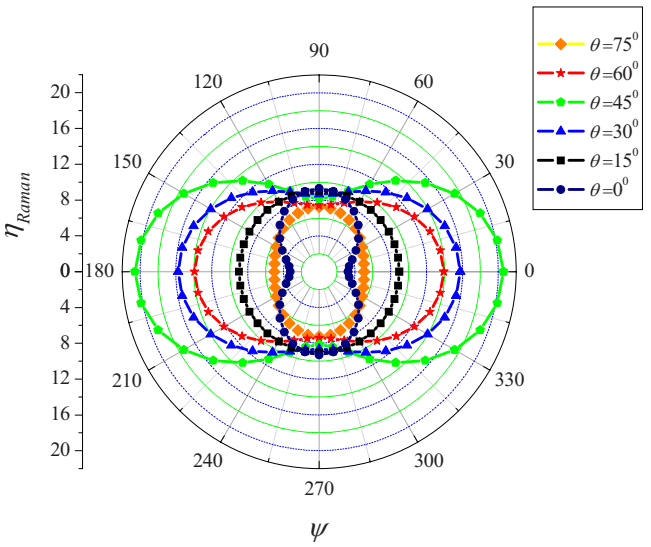

FIG. 6. (Color online) The polarization dependence SERS intensity at different incident angles $\theta=0°$ (navy filled circles), 15° (black filled squares), 30° (blue triangles), 45° (green pentagons), 60° (red stars), and 75° (orange diamonds), respectively. When the incident angles θ are smaller than 15°, the SERS intensity reaches a maximum at polarization angle of 90° and 270°. When the incident angles are bigger than 15°, the SERS intensity reaches a maximum at polarization angles of 0° and 180°.

ing Ag nanorod array (an ideal situation). In case (c), Eq. (32) will be simplified as

$$\eta_{\text{Raman}} = \frac{1}{2}[(1 + R_p + 2\sqrt{R_p}\cos\delta_p)^2 \sin^4(\theta_i) + 1]. \quad (33)$$

For each of these cases, we take $\tilde{n}_{\text{Ag}}=0.03+5.242i$, $\tilde{n}_{\text{glass}}=1.5$, and $\tilde{n}_{\text{vaccum}}=1$. Figure 5 shows the relationship between the relative Raman intensity η_{Raman} and the incident angles in the three cases with a fixed nanorod tilting angle $\beta=70°$. The excitation light is unpolarized. If the excitation light is normally incident onto the substrates, i.e., $\theta=0°$, the corresponding reflectances for the three different underlayers, Ag, glass, and air, are 0.9958, 0.04, and 0, respectively. The relative Raman intensity η_{Raman} obtained from Ag nanorod SERS substrates increases with the increase in reflectance from the underlayer, regardless of the incident angle. In case (a) the relative Raman intensity is about 800 times larger than that obtained from case (b) and is above 1200 times larger than that obtained from case (c). Therefore, the Ag thin-film layer scientifically improves the Raman intensity. This is quantitatively consistent with our experimental result,[34] which shows around 1000 times improvement compared Ag film with glass substrates. Figure 5 also shows that the SERS intensity-incident angle curves become narrower and narrower with the decrease in the reflectance of substrates, and the optimal incident angle becomes bigger and bigger: in case (a), the optimal incident angle $\theta_0=47°$; in case (b), $\theta_0=48°$; and in case (c), $\theta_0=58°$.

C. Effect of the polarization of the excitation light

The Ag nanorod SERS substrate has anisotropic morphology and is expected that the enhancement factor should depend on the excitation polarization. A SERS polarization dependence has been observed in our experiments.[37] To consider the effect of polarization dependence, one can decompose any arbitrary state of incident polarized light into $\vec{E}_p$ and $\vec{E}_s$. The angle, ψ, is the polarization angle between the electric-field direction and the p-polarization E-field direction. So $\langle E_{ip}^2\rangle=\langle E_i^2\rangle\cos^2\psi$ and $\langle E_{is}^2\rangle=\langle E_i^2\rangle\sin^2\psi$. The Raman scattering in case I can be only excited by the p-component of the E field, i.e., $\langle E_{\text{I}}^2\rangle$ corresponds to $\langle E_{Rp}^2\rangle$ and the scattering in case II can be only excited by the s component of the E field, i.e., $\langle E_{\text{II}}^2\rangle$ corresponds to $\langle E_{Rs}^2\rangle$. Thus, for the polarized incident light with polarization angle ψ, the relative Raman intensity η_{Raman} in Eq. (32) becomes

$$\begin{aligned}\eta_{\text{Raman}} &= A\cos^2\psi + B\sin^2\psi \\ &= \cos^2\psi\left[1 + R_p + \tilde{n}_2^4 R_p' + 2R_p^{1/2}\cos\delta_p\cos 2(\theta-\beta) + 2\tilde{n}_2^2 R_p^{1/2}\cos\left(\delta_p' + \frac{2\pi}{\lambda}\Delta\right)\sin 2\beta + 2\tilde{n}_2^2 R_p^{1/2} R_p'^{1/2}\sin 2\theta\right. \\ &\quad \left.\times\cos\left(\delta_p' + \frac{2\pi}{\lambda}\Delta - \delta_p\right)\right](1 + R_p + 2\sqrt{R_p}\cos\delta_p)\cos^2(\theta-\beta) + \sin^2\psi\left[1 + R_s' + 2\tilde{n}_2^2 R_s'^{1/2}\cos\left(\delta_s' + \frac{2\pi}{\lambda}\Delta\right)\right], \quad (34)\end{aligned}$$

where A and B are defined by Eqs. (27) and (30), respectively. Figure 6 shows the polarization angle ψ dependence of relative SERS intensity from the Ag nanorod substrate at different incident angles obtained from Eq. (34). In the calculations, the layer underneath is a Ag thin film with $\tilde{n}_2 = 0.03 + 5.242i$, and the incident angle is taken from 0° to 75° with 15° increment. At different incident angles, the shapes of the polarization dependent SERS intensity are different. If the incident angles are smaller than 15°, the maximum SERS intensity occurs at polarization angle of $\psi = 90°$ and $\psi = 270°$, which means most of the Raman scattering intensities observed are excited by the s-polarized component of the E field, i.e., the molecules shown in case II in Fig. 2. This is consistent with our experimental observation at $\theta = 0°$.[37] If the incident angle is larger than 15°, the SERS intensity reaches the maximum at polarization angles of $\psi = 0°$ and $\psi = 180°$, which means that most of the Raman scattering intensities collected are excited by the p-polarized component of the E field or the molecules shown in case I in Fig. 2. Note that, for any incident angle, the SERS intensities at the polarization angles of $\psi = 90°$ and $\psi = 270°$ are almost the same, since the Raman scattering only results from case II, which is independent of θ. However, the SERS intensity at $\psi = 0°$ and $\psi = 180°$ increases with the incident angle first, reaches a maximum at $\theta_0 = 45°$, and then decreases, which is consistent with Fig. 3.

IV. CONCLUSION

In summary, based on a modified Greenlner's model, the effect of incident angle, nanorod tilting angle, the underlayer thin film, and the polarization dependences of SERS obtained from Ag nanorod array substrates have been investigated. The results deduced from this simple model are quantitatively consistent with our experimental observations. (1) The SERS intensity is closely related to the incident angle and nanorod tilting angle. There is an optimal incident angle where the SERS intensity reaches its maximum. This optimal angle increases linearly with the nanorod tilting angle. (2) The underlayer thin-film reflection has a significant effect on the SERS intensity. The higher the reflectance is, the larger the SERS intensity is. (3) The SERS intensity is polarization dependent. For $\theta < 15°$, s-polarization excitation contributes more SERS intensity. For $\theta \geq 15°$, p-polarization excitation dominates the SERS intensity. The agreement between the model and experiments demonstrates that, although this is a crude model, it has captured the essential characteristics of the SERS for Ag nanorod array and can be used to guide further experimental development.

ACKNOWLEDGMENTS

Y.-J. Liu and Y.-P. Zhao acknowledge the support from National Science Foundation under Contract No. ECS-070178 and U.S. Army Research Laboratory under Grant No. W911NF-07–2–0065. The authors also acknowledge the fruitful discussions with Rich Dluhy. John Gibbs helped us to proofread the paper.

[1] J. M. Bello, V. A. Narayanan, D. L. Stokes, and T. Vo-Dinh, Anal. Chem. **62**, 2437 (1990).
[2] U. Brinkmann, Laser Focus World **40**, 15 (2004).
[3] K. I. Mullen and K. T. Carron, Anal. Chem. **63**, 2196 (1991).
[4] C. Viets and W. Hill, Sens. Actuators B **51**, 92 (1998).
[5] D. L. Stokes, Z.-H. Chi, and T. Vo-Dinh, Appl. Spectrosc. **58**, 292 (2004).
[6] J. A. Dieringer, A. D. McFarland, N. C. Shah, D. A. Stuart, A. V. Whitney, C. R. Yonzon, M. A. Young, X. Zhang, and R. P. Van Duyne, Faraday Discuss. **132**, 9 (2006).
[7] R. M. Jarvis and R. Goodacre, Anal. Chem. **76**, 40 (2004).
[8] W. R. Premasiri, D. T. Moir, M. S. Klempner, N. Krieger, G. Jones, and L. D. Ziegler, J. Phys. Chem. B **109**, 312 (2005).
[9] S. Shanmukh, L. Jones, J. D. Driskell, Y.-P. Zhao, R. A. Dluhy, and R. A. Tripp, Nano Lett. **6**, 2630 (2006).
[10] T. Vo-Dinh and D. L. Stokes, Field Anal. Chem. Technol. **3**, 346 (1999).
[11] T. Vo-Dinh, D. L. Stokes, G. D. Griffin, M. Volkan, U. J. Kim, and M. I. Simon, J. Raman Spectrosc. **30**, 785 (1999).
[12] X. Zhang, M. A. Young, O. Lyandres, and R. P. Van Duyne, J. Am. Chem. Soc. **127**, 4484 (2005).
[13] L.-P. Choo-Smith, H. G. M. Edwards, H. P. Endtz, J. M. Kros, F. Heule, H. Barr, J. S. Robinson, Jr., H. A. Bruining, and G. J. Puppels, Biopolymers **67**, 1 (2002).
[14] M. G. Shim and B. C. Wilson, J. Raman Spectrosc. **28**, 131 (1997).
[15] K. Katrin, K. Harald, I. Irving, R. D. Ramachandra, and S. F. Michael, J. Phys.: Condens. Matter **14**, R597 (2002).
[16] M. Fleischmann, P. J. Hendra, and A. J. McQuillan, Chem. Phys. Lett. **26**, 163 (1974).
[17] H. Xu, E. J. Bjerneld, M. Käll, and L. Börjesson, Phys. Rev. Lett. **83**, 4357 (1999).
[18] H. Xu, J. Aizpurua, M. Käll, and P. Apell, Phys. Rev. E **62**, 4318 (2000).
[19] M. I. Stockman, L. N. Pandey, and T. F. George, Phys. Rev. B **53**, 2183 (1996).
[20] S. Nie and S. R. Emory, Science **275**, 1102 (1997).
[21] K. Kneipp, Y. Wang, H. Kneipp, L. T. Perelman, I. Itzkan, R. R. Dasari, and M. S. Feld, Phys. Rev. Lett. **78**, 1667 (1997).
[22] N. P. Vitaliy and V. S. Tigran, J. Opt. A, Pure Appl. Opt. **8**, S208 (2006).
[23] A. Otto, I. Mrozek, H. Grabhorn, and W. Akemann, J. Phys.: Condens. Matter **4**, 1143 (1992).
[24] M. Moskovits, Rev. Mod. Phys. **57**, 783 (1985).
[25] M. Moskovits, J. Raman Spectrosc. **36**, 485 (2005).
[26] A. Campion and P. Kambhampati, Chem. Soc. Rev. **27**, 241 (1998).
[27] A. M. Polubotko, Opt. Commun. **127**, 135 (1996).
[28] K. T. Carron, G. Xue, and M. L. Lewis, Langmuir **7**, 2 (1991).
[29] V. L. Schlegel and T. M. Cotton, Anal. Chem. **63**, 241 (1991).
[30] B. Nikoobakht and M. A. El-Sayed, J. Phys. Chem. A **107**, 3372 (2003).

[31] A. Tao, F. Kim, C. Hess, J. Goldberger, R. He, Y. Sun, Y. Xia, and P. Yang, Nano Lett. **3**, 1229 (2003).
[32] C. L. Haynes and R. P. Van Duyne, J. Phys. Chem. B **105**, 5599 (2001).
[33] N. Felidj, J. Aubard, G. Levi, J. R. Krenn, A. Hohenau, G. Schider, A. Leitner, and F. R. Aussenegg, Appl. Phys. Lett. **82**, 3095 (2003).
[34] S. B. Chaney, S. Shanmukh, R. A. Dluhy, and Y.-P. Zhao, Appl. Phys. Lett. **87**, 031908 (2005).
[35] J. G. Fan and Y.-P. Zhao, J. Vac. Sci. Technol. B **23**, 947 (2005).
[36] Y.-J. Liu, J.-G. Fan, Y.-P. Zhao, S. Shanmukh, and R. A. Dluhy, Appl. Phys. Lett. **89**, 173134 (2006).
[37] Y.-P. Zhao, S. B. Chaney, S. Shanmukh, and R. A. Dluhy, J. Phys. Chem. B **110**, 3153 (2006).
[38] R. N. Tait, T. Smy, and M. J. Brett, Thin Solid Films **226**, 196 (1993).
[39] L. Abelmann and C. Lodder, Thin Solid Films **305**, 1 (1997).
[40] Y.-P. Zhao, D.-X. Ye, G.-C. Wang, and T.-M. Lu, Proc. SPIE **5219**, 15 (2003).
[41] Y.-P. Zhao, S. Shanmukh, Y.-J. Liu, S. B. Chaney, L. Jones, R. A. Dluhy, and R. A. Tripp, Proc. SPIE **6324**, 63240M (2006).
[42] J. D. Driskell, S. Shanmukh, Y.-J. Liu, S. B. Chaney, X. J. Tang, Y.-P. Zhao, and R. A. Dluhy, J. Phys. Chem. C **112**, 895 (2008).
[43] R. G. Greenler and T. L. Slager, Spectrochim. Acta, Part A **29**, 193 (1973).
[44] A. Campion, in *Vibrational Spectroscopy of Molecules on Surface*, edited by J. T. Yates, Jr. and T. E. Madey (Plenum, New York, 1987).
[45] Z. Y. Zhang and Y.-P. Zhao, Appl. Phys. Lett. **89**, 023110 (2006).
[46] W.-h. Yang, J. Hulteen, G. C. Schatz, and R. P. Van Duyne, J. Chem. Phys. **104**, 4313 (1996).
[47] A. G. Dirks and H. J. Leamy, Thin Solid Films **47**, 219 (1977).